

Observations and analysis of an urban boundary layer and sea breezes during extreme heat events

Gabriel Rios ^{1*}, ^{2*}, Prathap Ramamurthy ^{1, 2}

1. Department of Mechanical Engineering, CUNY City College, New York, New York
2. NOAA Center for Earth System Sciences and Remote Sensing Technologies, New York, New York

Corresponding author: Gabriel Rios (grios001@citymail.cuny.edu)

*** Current affiliation(s):** Department of Mechanical Engineering, CUNY City College, New York, New York; NOAA Center for Earth System Sciences and Remote Sensing Technologies, New York, New York

For submission to the Quarterly Journal of the Royal Meteorological Society.

Last updated: February 14, 2022.

1 Abstract

Extreme heat presents a significant risk to human health and infrastructure in cities. Several studies have been conducted in the past several decades to understand the interaction between the synoptic-scale extreme heat events and local-scale urban heat island effects. However, observations of boundary layer characteristics during these periods have been relatively rare. Our current understanding of urban boundary layer structure is incomplete, particularly in coastal environments where the local climatology is highly influenced by land-sea thermal gradients. In this study, we analyze the evolution and structure of the urban boundary layer during regular and extreme heat periods with the goal of better understanding the effect of extreme heat and sea breezes on the boundary layer over a coastal urban area. Our analysis focuses on the New York City metropolitan area and relies on observations from vertical profilers (Doppler lidar, microwave radiometer) and quantities derived by analytical methods. Additionally, satellite and reanalysis data are used to supplement observational data. Extreme heat events present a mean peak surface temperature increase of 7K, an increase of site-averaged specific humidity at the surface by 39.4%, and a marked southwesterly shift in winds at all sites. In addition, sea breeze events during heat extreme heat events are found to reduce temperatures and increase low-level moisture content from the early evening through nighttime hours, with strong variability between sites. The study also finds that extreme heat events unify horizontal wind directions throughout the boundary layer, and promote nocturnal onshore moisture transport.

19 1 Introduction

Extreme heat poses a major risk to life and property. The effects of extreme heat are expected to impact cities especially, which presents a significant hazard for vulnerable populations and infrastructure. With regards to effects on public health, studies have shown that extreme and prolonged heat increases mortality and exacerbates existing health conditions in high-risk populations (Anderson and Bell, 2011; Frumkin, 2016; Heaviside, Macintyre, and Vardoulakis, 2017; Madrigano et al., 2015). With regards to effects on infrastructure, studies have shown that extreme heat subjects networks critical to urban areas (e.g., electrical grid, public transportation) under significant stresses and/or failure (McEvoy, Ahmed, and Mullett, 2012; Zuo et al., 2015). These events are projected to increase in frequency due to the effects of climate change. Projections indicate that the impacts of future climate will cause adverse effects of extreme heat to become more frequent and severe (Burillo et al., 2019; Forzieri et al., 2018; Peng et al., 2011).

31 The meteorology of extreme heat events and its impacts on urban areas can be observed from the synoptic
32 and local scales. From a synoptic scale, extreme heat events are often caused by the sustained presence of
33 a high-pressure system over an area, resulting in lower wind speeds and warm air subsidence, promoting
34 higher surface temperatures (Black et al., 2004; Miralles et al., 2014). From a local perspective, the
35 amplified impact of extreme heat events on cities is a result of the urban heat island (UHI) effect,
36 which occurs as a result of the modification of land surface properties due to the built environment.
37 The modification of surface properties has been shown to increase near-surface air temperatures due
38 to factors such as radiation entrapment, increased heat storage, and lower evapotranspirative cooling
39 (Chen, Yang, and Zhu, 2014; Li and Elie Bou-Zeid, 2013; Ramamurthy and Bou-Zeid, 2017; Zhao et
40 al., 2018). Additionally, urban areas near large bodies of water experience effects from the sea breeze,
41 which has been shown to play a moderating influence on the intensity of the UHI effect (Hu and Xue,
42 2016; Jiang et al., 2019; Stéfanon et al., 2014). The processes on these two scales can be connected by
43 understanding the structure and dynamics of the urban boundary layer (UBL), which is the lowest part of
44 the troposphere in which surface-atmosphere exchanges occur that directly affect human activity. There
45 have been a large number of numerical studies performed to improve our understanding of UBL processes
46 during extreme heat events, which have been important for conceptualizing the role of synoptic-scale
47 and surface forcings on urban climate. Something about the vertical structure of the UBL and coupling
48 these

49 However, detailed observational analyses of UBL structure and dynamics are somewhat limited, especially
50 in the vertical direction. Over the last 20 years, microwave radiometers, lidars, and radiosondes have
51 been shown to be essential for accomplishing this. Microwave radiometers have been used to determine
52 vertical profiles of temperature and water vapor (Rose et al., 2005; Z. Wang et al., 2012), while lidars
53 being used to observe three-dimensional wind fields and aerosol concentrations (Grund et al., 2001).
54 Although radiosondes provide direct measurements of the aforementioned properties in the boundary
55 layer as it moves vertically through it, they present greater difficulties (e.g., cost, shorter supply) and
56 are unable to observe at the temporal resolution of microwave radiometers and lidars.

57 Although somewhat limited in spatiotemporal scale, numerous observational campaigns have been per-
58 formed to better our understanding of UBL structure and dynamics. Barlow et al. (2011) provides an
59 in-depth study of boundary layer dynamics above London over a month-long period using a combination
60 of a sonic anemometer and Doppler lidar, allowing for high-resolution vertical observations of a complex
61 UBL and a better understanding of turbulent structures and vertical mixing processes. Similarly, Pel-
62 liccioni et al. (2012) employs a sonic anemometer and a sodar system at a site in Rome to observe and
63 analyze the lower 200 m of the UBL to determine UBL characteristics and explore the validity of Monin-
64 Obukhov similarity theory in the surface layer. Additionally, Arruda Moreira et al. (2020) evaluates the
65 ability of lidar and microwave radiometer systems to observe turbulence over a variety of atmospheric
66 conditions, including the effects of significant dust concentrations, in the region around Granada, Spain.
67 Studies such as those performed by Banks et al. (2015), Quan et al. (2013), and Z. Wang et al. (2012)
68 further demonstrate the ability of vertical profiling instruments to analyze the boundary layer structure
69 by deriving UBL heights and its diurnal evolution. Expanding upon UBL structure, Anurose, Subra-
70 hamanyam, and Sunilkumar (2018) details a long-term observational campaign over an urban location
71 in southern India that chronicles UBL height through monsoon season, annual averages of near-surface
72 quantities, and the dynamics and effects of the sea breeze circulation.

73 Observations of the UBL during extreme heat events are even more limited. Ramamurthy and Bou-Zeid
74 (2017) used microwave radiometers to observe the UBL over New York City in July 2016 to find that the
75 UHI effect was amplified during heat wave events and that spatial variability throughout the city was
76 significant throughout the observation period. Jiang et al. (2019) explores the effects of heat waves on
77 rural and urban areas for several cities in China using ground-based observations with a focus on the UHI
78 effect, finding that the effect was amplified during heat waves due to greater surface solar radiation and

shifts in wind direction contributing to advection of heated air masses over the studied cities. (Wu et al., 2019) uses a combination of a ceilometer and multiple lidars to observe the evolution of UBL structure, air quality, and pollutant transport during a heat wave in New York City, demonstrating sharp rates of UBL growth due to convective activity and an increase of pollutant concentration and regional transport. Zhang et al. (2020) uses aircraft-based observations to provide a comprehensive analysis of UBL structure during heat wave events over cities in the United States throughout a 10-year period, providing insights into the 'heat dome' thermodynamic structure over cities and the variability between heat wave events due to local (such as surface properties in urban areas) and large-scale (such as synoptic meteorological conditions) forcings.

New York City represents a complex case for urban meteorology given its diverse array of land cover types (deciduous forest to supertall skyscrapers) and its proximity to multiple major bodies of water (Lower New York Bay and the New York Bight to the south and east, Long Island Sound to the north and east). Due to these factors, the effects of the surface energy budget (Hrisko, Prathap Ramamurthy, and Gonzalez, 2021; Prathap Ramamurthy and Bou-Zeid, 2014; Tewari et al., 2019) and sea breezes (Childs and Raman, 2005; Colle and Novak, 2010; Frizzola and Fisher, 1963; Gedzelman et al., 2003; Melecio-Vázquez et al., 2018; Thompson, Holt, and Pullen, 2007) on the mesoscale meteorology have been studied extensively. However, similar to studies of other urban areas mentioned previously, much of this research has involved numerical simulations of these meteorological processes. In this study, we attempt to further our understanding of the UBL over a coastal urban area by compiling observations from multiple locations within New York City and analyzing the UBL using derived quantities.

This study attempts to use observations and analytical methods to provide insight into the following questions:

1. How do UBL structure and dynamics depart from the climatology during extreme heat events?
2. How do extreme heat events impact the transport of scalars?
3. What effect does the sea breeze have on a coastal urban area during extreme heat events?

2 Data collection and analysis

2.1 Study site

The UBL over New York City is observed and analyzed in this study. Observational data was captured at four locations within New York City (Table 1).

Table 1: Locations and details of observations sites.

	Bronx	Queens	Staten Island
Coordinates	40.87248°N, 73.89352°E	40.73433°N, 73.81585°E	40.60401°N, 74.14850°E
Elevation (m a.g.l.)	57.8	56.3	32.4
Element roughness height (m a.g.l.)			
Valid wind directions	N/A	180 to 360°	N/A

2.2 Observational instruments

Observations of the UBL were made using a synthesis of microwave radiometers, lidars, and satellites. Vertical profiles of temperature and vapor density were captured using a network of Radiometrics MP-3000A microwave radiometers (Hewison and Gaffard, 2003) operated by the New York State

114 Mesonet (Brotzge et al., 2020). Profiles for water vapor are retrieved using 21 channels in the 22-30.0
115 GHz (K-band) range, while profiles for temperature are retrieved using 14 channels in the 51-59.0 GHz
116 (V-band) range. Profile accuracy (relative to radiosonde soundings) determined by performance studies
117 at various locations reported an annually-averaged water vapor accuracy within 1.0 g m^{-3} below 2 km
118 and an annually-averaged temperature accuracy within 1.6 K below 4 km (Güldner and Spänkuch, 2001;
119 Sánchez et al., 2013). Quantities are captured at 58 height levels starting at ground level and ending
120 at 10 km above ground level, with vertical steps of 50 m from ground level to 500 m, 100 m from 500 m
121 to 2 km, and 250 m steps above 2 km. Observation integration times range from 0.01 to 2.50 s. Vertical
122 profiles are generated every 10 s and averaged over 10 min periods.

123

124 Wind measurements were measured using a network of Leosphere WindCube 100S Doppler lidars
125 operated by the New York State Mesonet (Brotzge et al., 2020). Measurements of wind motion using
126 the Doppler beam swinging scan mode in three directions: zonal (u), meridional (v), and vertical (w)
127 over 20 s cycles, with measurements averaged over 10 min intervals (Shrestha et al., 2021). The vertical
128 range of the WindCube 100S is 7 km above ground level with wind speed and direction accuracies of
129 0.5 m s^{-1} and 2° , respectively. The WindCube 100S has also been shown to perform with a high degree
130 of accuracy relative to radiosonde soundings, especially above 500 m (Kumer, Reuder, and Furevik, 2014).

131

132 Land and sea surface temperatures were estimated using derived products from the NOAA/NASA
133 GOES-16 Advanced Baseline Imager (ABI) (Ignatov et al., 2010; Yu et al., 2008). The GOES-16 ABI
134 provides a spatial resolution of 2 km with real-time data available to the public on an hourly basis.
135 The spatial extent of the Land Surface Temperature (LST) product ranges from the continental United
136 States (CONUS) to the majority of the Western Hemisphere (known as *full disk*), whereas the Sea
137 Surface Temperature (SST) product has a full disk spatial extent. The LST product has been found
138 to have an error relative to surface observations of 2.5 K over all land cover types, while sea surface
139 temperatures (SSTs) estimated using the GOES-16 ABI have been found to have an error relative to
140 shipborne radiometers $\leq 1 \text{ K}$ in the New York Bight (Luo and Minnett, 2021).

141 2.2.1 Data criteria & availability

142 Dates selected for this study are categorized into three groups: (1) normal days, (2) extreme heat days,
143 and (3) sea breeze days. For the purposes of this study, *extreme heat events* are defined as 3 or more
144 consecutive days with maximum daily temperatures exceeding 90°F (305 K), per the New York branch
145 of NOAA National Weather Service (Robinson, 2001; National Weather Service, 2018), while *normal*
146 *days* are defined as days that do not meet these criteria. Because the aim of this study is to observe the
147 effect of extreme heat on the UBL, normal day selection was restricted to months in which extreme heat
148 events occurred (May through September), as well as days in which 50% or more of the day featured
149 clear-sky conditions below 3.65 km above ground level due to the association of extreme heat events with
150 reduced daytime cloud coverage and precipitation (Stéfanon et al., 2014; Thomas et al., 2020). Clear-
151 sky conditions were identified by using an average of 5-minute surface-based observations from three
152 airports in the Automated Surface Observation System (ASOS) (NOAA et al., 1998) network within
153 the New York City metropolitan area: Newark Liberty International Airport (EWR), John F. Kennedy
154 International Airport, and LaGuardia Airport. *Sea breeze events* are identified as times during normal
155 and extreme heat days in which the low-level ($\leq 200 \text{ m}$) mean horizontal wind speed (U) is less than
156 5 m s^{-1} and low-level wind direction has a primarily easterly component, due to the presence of the
157 Atlantic Ocean to the east of New York City.

158 - Discuss quality filtering - Plots showing sampling counts per hour per site per day

159 **2.3 Derived quantities**

160 **3 Normal and extreme heat boundary layer properties**

161 This section discusses the differences in boundary layer structure and properties between normal days
162 and extreme heat events. Results are presented from the averages over all identified normal and heat
163 event days.

164 **3.1 Temperature**

165 On average, extreme heat events increase the temperature at the surface, as expected (see Figure
166 4). This is consistent across all observed locations in New York City, with the extreme heat event
167 temperature exceeding normal temperatures by approximately $1-\sigma$ over the entire day. An increase in
168 the difference is observed during daytime hours, with the difference peaking in magnitude around 13:00
169 LST at the hottest time of day. The surface temperature variability is significantly lower during heat
170 events (average $\sigma = 1.77\text{K}$) than during normal temperatures (average $\sigma = 4.57\text{K}$). There is little
171 spatial variability between sites, with maximum average temperatures ranging from 305.65 K in Queens
172 to 306.63 K in the Bronx. It is worth noting that there are areas in New York City that are located
173 in more heavily urbanized areas than the observation sites (such as Midtown Manhattan and central
174 Brooklyn), so it is likely that certain areas within the city have higher maximum temperatures.

175
176 Above the surface, extreme heat events increase the temperature significantly over the lowest
177 3000 m of the troposphere (see Figure 3), with standardized anomalies of θ ranging from $\sigma = 0.99$ to
178 1.30. The largest temperature anomalies shift from the surface layer in the mornings to span the entirety
179 of the mixed layer. This is reflective of strong surface forcing resulting in convection through the mixed
180 layer, as indicated by the formation of a late morning superadiabatic layer at all locations (Figures 5, 6, 7).

181
182 These vertical profiles of θ suggest a degree of spatial variability in the UBL exists between loc-
183 ations. One instance of this spatial variability is vertical mixing; the Bronx site appears to have
184 stronger vertical mixing as shown in Figure 5, as θ remains constant for a greater height than at
185 the Queens and Staten Island locations, indicating a deeper mixed layer. This phenomenon is more
186 pronounced during extreme heat events, as a distinct mixed layer is apparent in the Bronx during early
187 (12:00 LST) and late (18:00 LST) afternoon hours. While a deepened mixed layer during extreme heat
188 events is also visible for the other locations, the strength of vertical mixing in the Bronx is emphasized
189 by persistent afternoon instability as shown by negative $\frac{d\theta}{dz}$ values between 500 and 1000 m and a
190 superadiabatic surface layer and 12:00 and 18:00 LST.

191 **3.2 Moisture**

192 On average, extreme heat events were found to increase the moisture at the surface, as indicated by
193 the diurnal profiles of specific humidity (q) (see Figure 9). This is also consistent across all observed
194 locations in New York City, with the extreme heat event temperature exceeding normal temperatures
195 by approximately $1-\sigma$ over the entire day. Although a distinct diurnal profiles exists (q decreases during
196 daytime hours), the diurnal range is smaller in magnitude than temperature. It is also worth noting
197 that the diurnal range is lower for Staten Island than for the Bronx or Queens, suggesting that degree of
198 urbanization has a negative correlation with the diurnal range of q . Similar to surface temperature, the
199 variability of q is significantly lower during heat events (average $\sigma = 2.14 \times 10^{-3} \text{ kg kg}^{-1}$) than during
200 normal temperatures (average $\sigma = 3.18 \times 10^{-3} \text{ kg kg}^{-1}$). Queens shows exceptional variability in q ,
201 which may be attributed to the location of the observation site, which is adjacent to Flushing Meadows
202 Corona Park (large open vegetated space), is surrounded by a medium-density urban area on all other
203 sides, and is approximately 4 km from Long Island Sound.

204

205 In the boundary layer, the positive q anomalies subside in magnitude between 300 and 600 m,
 206 but increase significantly in the mixed layer, especially during the late morning and early afternoon for
 207 all sites. As shown in Figure 8, the largest anomalies occur between 10:00 and 16:00 LST throughout the
 208 mixed layer. With regards to spatial variation in q , Staten Island demonstrates a strong positive anomaly
 209 overnight through the early morning near the surface, indicating elevated low-level moisture transport
 210 during extreme heat events, whereas the Bronx and Queens demonstrate a similar phenomenon with
 211 a lesser anomaly magnitude. All sites show significant positive q anomalies throughout the day, with
 212 the strongest anomaly signal starting in the low-levels throughout the morning and transitioning to the
 213 mixed later by mid-afternoon. This trend suggests that the increase in nocturnal low-level moisture
 214 corresponds to increased UBL moisture content due to strong vertical mixing throughout the daytime.

215

216 This is supported by Figures 10, 11, 12, where vertical profiles of q across all locations show
 217 markedly higher q values at the surface during extreme heat events with $\frac{dq}{dz}$ values increasing throughout
 218 the morning in the mixed layer while low-level q values decrease, indicating vertical transport of moisture
 219 and drier low-level conditions during peak insolation. The strong vertical mixing of q can be observed
 220 at all sites, where late morning and early afternoon $\frac{dq}{dz}$ values are greater during extreme heat events
 221 than normal days. An example can be seen in the Bronx, where $\frac{dq}{dz} > 0$, indicating very efficient vertical
 222 moisture transport.

223 3.3 UBL dynamics

224 3.3.1 Horizontal winds

225 Extreme heat events coincided with an overall reduction of horizontal wind speeds (U) in the UBL. More
 226 specifically, the magnitude of U during extreme heat events is similar in magnitude to U during normal
 227 days with the exception of early morning hours and at upper levels of the UBL. As shown in Figure
 228 13, modest reductions in U ($-1.2 \leq \sigma \leq -0.4$) during extreme heat events are present throughout the
 229 UBL from early to mid-morning, with little differences throughout the rest of the day ($-0.4 \leq \sigma \leq 0.4$).
 230 Larger deviations between U values are present at the top of the UBL where synoptic conditions become
 231 dominant.

232

233 Vertical profiles of U for normal and extreme heat events provide a more detailed view of the
 234 differences in UBL structure. Across all sites, U is similar throughout the UBL overnight, afternoon,
 235 and evenings. During early morning hours, extreme heat event U values decrease by 25 to 50%
 236 throughout the entire UBL (see Figures 15, 16, 17), although both event types present a classical
 237 logarithmic wind profile, with surface friction effects present through 500 m. Another phenomenon
 238 worth noting is the difference in U profiles above 2000 m; profiles of U during extreme heat events
 239 are more consistent between sites and vertically than during normal days. This phenomenon may
 240 highlight the effect of synoptic meteorological conditions on U , as the UBL typically remains below
 241 2500 m. During extreme heat events, anticyclonic conditions produce more stable atmospheric con-
 242 ditions relative to normal days, resulting in less variability between heat events than during normal days.

243

244 Extreme heat events result in a southwesterly shift in U throughout the UBL. This shift is present most
 245 evidently closer to the surface, as shown in Figures 18, 19, and 20, with winds at 100 m coming primarily
 246 from the southwest quadrant. Figure 19 shows that Queens also presents a secondary maximum with
 247 winds approaching from the south, which suggests effects from the Atlantic sea breeze (effects from
 248 the sea breeze will be further discussed in Section 4). At 1000 m, the directionality of prevailing winds
 249 becomes more uniform between normal and extreme heat days, as winds primarily approach New
 250 York City from the west-southwest. The disparity in wind directions between 100 and 1000 m suggests
 251 that localized wind fields play a major role in UBL dynamics at lower levels whereas synoptic-scale

252 atmospheric conditions increasingly dominate with increasing height.

253 **3.3.2 Vertical motion**

254 On average, extreme heat events do not appear to produce significant changes in vertical velocity (w).
255 Figure 21 shows average diurnal profiles of w at all locations at 100 m above ground level, with similar
256 mean values throughout the day between normal days and extreme heat events. During extreme heat
257 events, however, the variability of w is less in the early morning hours and greater in the evening. This
258 phenomenon is also observed in vertical profiles of w at all locations as shown in Figures 23, 24, and
259 25. At all locations, overnight and morning profiles of w (0:00 and 6:00 LST) show significantly lower
260 variability in w throughout the UBL with similar magnitudes of mean w . Despite similar means and
261 deviations in the early afternoon (12:00 LST), evening profiles (18:00 LST) show significantly higher
262 variability in w below 500 m for all sites, with the Bronx showing this occurrence extend through the
263 UBL.

264 **4 Effects of the sea breeze circulation**

265 Sea breezes in New York City occur as a result of land-sea temperature gradients from two arms of the
266 Atlantic Ocean; the New York Bight to the southeast and Long Island Sound to the northeast. Sea
267 breezes from both bodies increase the complexity of UBL dynamics over New York City due to the
268 coalescence of opposing fronts over a complex topography (Bornstein and Thompson, 1981). A typical
269 sea breeze event in New York City is defined by calm ambient low-level winds ($\leq 5 \text{ m s}^{-1}$, the formation
270 of a large land-sea temperature gradient in the mid- to late morning, strong late-morning thermals that
271 promote low-level convergence, and afternoon to early-evening onshore moisture transport and reduction
272 in surface air temperatures (especially in areas closest to the shore) (Childs and Raman, 2005; Frizzola
273 and Fisher, 1963; Gedzelman et al., 2003).

274 Sea breeze events occurred on approximately 56% of all days observed. The high frequency of occurrence
275 is likely attributable to the large land-sea temperature gradient that is common during warmer months
276 (Gedzelman et al., 2003), as days were chosen exclusively between May and September. Maximum land-
277 sea surface temperature differences during days with identifiable sea breeze events averaged at 12 K, with
278 a strong diurnal profile with the peak difference occurring around midday (see Figure 26). The frequency
279 of occurrence increases when observing days during extreme heat events, as the lack of a strong synoptic
280 wind allows for the sea breeze circulation to become dominant in the metropolitan area (Miller et al.,
281 2003).

282 **4.1 UBL structure during sea breeze events**

283 During normal days, observations show that the sea breeze reduces temperatures and increases moisture
284 content throughout the UBL after 12:00 LST. In Figure 27, the standardized anomalies of θ between
285 normal days with and without a sea breeze are shown, averaged over all days for each set of days.
286 Overnight and in the early morning, positive anomalies of θ are present above the UBL ($\leq 1 \text{ km}$)
287 until mid-morning, with the Bronx having the most significant anomaly and Staten Island the least.
288 This suggests a decreasing degree of anomalous θ with decreasing urbanization. This anomaly pattern
289 coincides with a positive q anomaly trend in both the spatiotemporal aspect (peak anomaly occurs
290 above 1 km before 8:00 LST) and the magnitude aspect (the Bronx has the most significant early
291 morning anomaly, Staten Island has the least). Later in the day, all sites observe a negative θ anomaly
292 throughout the UBL despite a negative q anomaly, indicating that sea breeze events during normal
293 days coincide with a cooler and drier daytime UBL. Sea breeze effects become apparent during the
294 mid-afternoon with the presence of a significant negative θ and positive q anomaly in the lower UBL,
295 with Staten Island experiencing effects first (approximately 16:00 LST) and the Bronx experiencing
296 effects last. It is worth noting that the q anomaly is weakest in the Bronx, indicating that the sea breeze

297 front weakens as it travels inland over New York City.

298

299 During extreme heat events, observations show that the sea breeze plays a moderating role on
300 surface conditions by reducing low-level temperatures and increasing low-level moisture content, similar
301 to phenomena observed during normal days. In Figure 29, the standardized anomalies of θ between
302 extreme heat days with and without a sea breeze are shown, averaged over all days. All sites shown
303 that extreme heat days with a sea breeze possess slightly higher values of θ in the mid-morning,
304 with significant low-level reduction in θ in the afternoon and evening. On average, the onset of the
305 low-level cooling occurs in Staten Island first at approximately 12:00 LST, with Queens following at
306 approximately 14:00 LST, and the Bronx at about 18:00 LST. This disparity in times appears to
307 represent the passage of the southeasterly sea breeze front through New York City, where the onset
308 time correlates with the distance from the New York Bight (Bornstein and Thompson, 1981). A similar
309 phenomenon is observed by the transport of q as shown in Figure 30, with drier conditions throughout
310 the UBL before 12:00 LST and increasing low-level moisture as the day progresses. With regards to
311 onset, q follows a similar pattern to θ in that the onset time is dependent from distance to the shore.
312 These anomalies present most significantly in the lowest 1000 m of the UBL after 12:00 LST, which
313 aligns with sea breeze circulation characteristics observed in Frizzola and Fisher (1963).

314 4.2 UBL dynamics during sea breeze events

315 Days with identifiable sea breeze events had lower U throughout the majority of the UBL, with the most
316 significant decreases during the nighttime, potentially due to the lessening of onshore flow due to the
317 reduction of the land-sea temperature gradient (Pullen et al., 2007), as shown in Figure 26. Vertical
318 motions, however, increased significantly in the Bronx and Queens during the late morning and early
319 afternoon, as shown in Figure 31. These anomalies likely indicate the increased presence of updrafts in
320 urbanized areas.

321 During days with identified sea breeze circulations, easterly winds increase in frequency in the lower
322 levels of the UBL, as shown in Figures 32, 33, and 34. Southeasterly winds (due to sea breezes from
323 the New York Bight) increased in frequency compared to all other days at all locations. The occurrence
324 frequency of southeasterly winds is correlated with the distance between the observation site and the
325 largest body of water in proximity of the metropolitan area (Atlantic Ocean), as Staten Island reported
326 92.1% of all winds at 100 m as southeasterly between 12:00 and 20:00 LST (distance of 6.50 km from
327 Lower New York Bay), whereas Queens reported 67.4% (distance of 16.5 km), and Bronx reported 55.6%
328 (distance of 32.9 km).

329 For sites near Long Island Sound (the Bronx and Queens), northeasterly winds increased in frequency
330 as well, though not to the same magnitude as southeasterly winds. This disparity in magnitude suggests
331 that the Long Island Sound sea breeze front is weaker than the New York Bight sea breeze front, which
332 aligns with previous studies of sea breeze fronts over New York City (Frizzola and Fisher, 1963; Meir
333 et al., 2013).

334 5 Conclusions

- 335 • How do UBL structure and dynamics depart from the climatology during extreme heat events?
- 336 • How does the UBL structure impact the transport of scalars?
- 337 • The sea breeze reduces temperatures throughout the UBL after the onset of the sea breeze, which
338 typically occurs in the mid-afternoon in immediate coastal areas and in the evening for areas
339 further inland. The sea breeze also results in nocturnal low-level onshore moisture transport.

340 Acknowledgments

341 This research is made possible by the New York State (NYS) Mesonet. Original funding for the NYS
342 Mesonet was provided by Federal Emergency Management Agency grant FEMA-4085-DR-NY, with the
343 continued support of the NYS Division of Homeland Security & Emergency Services; the state of New
344 York; the Research Foundation for the State University of New York (SUNY); the University at Albany,
345 SUNY; the Atmospheric Sciences Research Center (ASRC) at SUNY Albany; and the Department of
346 Atmospheric and Environmental Sciences (DAES) at SUNY Albany.

347 References

- 348 Anderson, G Brooke and Michelle L Bell (2011). "Heat waves in the United States: mortality risk during heat
349 waves and effect modification by heat wave characteristics in 43 US communities". In: *Environmental health
350 perspectives* 119.2, pp. 210–218.
- 351 Anurose, TJ, D Bala Subrahmanyam, and SV Sunilkumar (2018). "Two years observations on the diurnal
352 evolution of coastal atmospheric boundary layer features over Thiruvananthapuram (8.5° N, 76.9° E), India".
353 In: *Theoretical and applied climatology* 131.1, pp. 77–90.
- 354 Arruda Moreira, Gregori de et al. (2020). "Study of the planetary boundary layer height in an urban environment
355 using a combination of microwave radiometer and ceilometer". In: *Atmospheric Research* 240, p. 104932.
- 356 Banks, Robert F et al. (2015). "Performance evaluation of the boundary-layer height from lidar and the Weather
357 Research and Forecasting model at an urban coastal site in the north-east Iberian Peninsula". In: *Boundary-
358 layer meteorology* 157.2, pp. 265–292.
- 359 Barlow, Janet F et al. (2011). "Boundary layer dynamics over London, UK, as observed using Doppler lidar
360 during REPARTEE-II". In: *Atmospheric Chemistry and Physics* 11.5, pp. 2111–2125.
- 361 Black, Emily et al. (2004). "Factors contributing to the summer 2003 European heatwave". In: *Weather* 59.8,
362 pp. 217–223.
- 363 Bornstein, Robert D and William T Thompson (1981). "Effects of frictionally retarded sea breeze and synoptic
364 frontal passages on sulfur dioxide concentrations in New York City". In: *Journal of Applied Meteorology and
365 Climatology* 20.8, pp. 843–858.
- 366 Brotzge, Jerald A et al. (2020). "A technical overview of the new york state mesonet standard network". In:
367 *Journal of Atmospheric and Oceanic Technology* 37.10, pp. 1827–1845.
- 368 Burillo, Daniel et al. (2019). "Electricity infrastructure vulnerabilities due to long-term growth and extreme heat
369 from climate change in Los Angeles County". In: *Energy Policy* 128, pp. 943–953.
- 370 Chen, Feng, Xuchao Yang, and Weiping Zhu (2014). "WRF simulations of urban heat island under hot-weather
371 synoptic conditions: The case study of Hangzhou City, China". In: *Atmospheric research* 138, pp. 364–377.
- 372 Childs, Peter P and Sethu Raman (2005). "Observations and numerical simulations of urban heat island and sea
373 breeze circulations over New York City". In: *Pure and Applied Geophysics* 162.10, pp. 1955–1980.
- 374 Colle, Brian A and David R Novak (2010). "The New York Bight jet: climatology and dynamical evolution". In:
375 *Monthly Weather Review* 138.6, pp. 2385–2404.
- 376 Forzieri, Giovanni et al. (2018). "Escalating impacts of climate extremes on critical infrastructures in Europe".
377 In: *Global environmental change* 48, pp. 97–107.
- 378 Frizzola, John A and Edwin L Fisher (1963). "A series of sea breeze observations in the New York City area".
379 In: *Journal of Applied Meteorology and Climatology* 2.6, pp. 722–739.
- 380 Frumkin, Howard (2016). "Urban sprawl and public health". In: *Public health reports*.
- 381 Gedzelman, SD et al. (2003). "Mesoscale aspects of the urban heat island around New York City". In: *Theoretical
382 and applied climatology* 75.1, pp. 29–42.
- 383 Grund, Christian J et al. (2001). "High-resolution Doppler lidar for boundary layer and cloud research". In:
384 *Journal of Atmospheric and Oceanic Technology* 18.3, pp. 376–393.
- 385 Güldner, J and D Späckkuch (2001). "Remote sensing of the thermodynamic state of the atmospheric boundary
386 layer by ground-based microwave radiometry". In: *Journal of Atmospheric and Oceanic Technology* 18.6,
387 pp. 925–933.
- 388 Heaviside, Clare, Helen Macintyre, and Sotiris Vardoulakis (2017). "The urban heat island: implications for health
389 in a changing environment". In: *Current environmental health reports* 4.3, pp. 296–305.

- 390 Hewison, Tim and Catherine Gaffard (2003). "Radiometrics MP3000 microwave radiometer performance assessment". In: *Obs. Development Technical Report TR29, Met Office, National Meteorological Library, Exeter, UK. Also available from <http://tim.hewison.org/TR29.pdf>.*
- 391
- 392
- 393 Hrisko, Joshua, Prathap Ramamurthy, and Jorge E Gonzalez (2021). "Estimating heat storage in urban areas using multispectral satellite data and machine learning". In: *Remote Sensing of Environment* 252, p. 112125.
- 394
- 395 Hu, Xiao-Ming and Ming Xue (2016). "Influence of synoptic sea-breeze fronts on the urban heat island intensity in Dallas–Fort Worth, Texas". In: *Monthly Weather Review* 144.4, pp. 1487–1507.
- 396
- 397 Ignatov, A et al. (2010). "GOES-R Advanced Baseline Imager (ABI) algorithm theoretical basis document for sea surface temperature". In: *NOAA NESDIS Center for Satellite Applications and Research*.
- 398
- 399 Jiang, Shaojing et al. (2019). "Amplified urban heat islands during heat wave periods". In: *Journal of Geophysical Research: Atmospheres* 124.14, pp. 7797–7812.
- 400
- 401 Kumer, Valerie-M, Joachim Reuder, and Birgitte R Furevik (2014). "A comparison of LiDAR and radiosonde wind measurements". In: *Energy Procedia* 53, pp. 214–220.
- 402
- 403 Li, Dan and Elie Bou-Zeid (2013). "Synergistic interactions between urban heat islands and heat waves: The impact in cities is larger than the sum of its parts". In: *Journal of Applied Meteorology and Climatology* 52.9, pp. 2051–2064.
- 404
- 405 Luo, Bingkun and Peter J Minnett (2021). "Skin Sea Surface Temperatures From the GOES-16 ABI Validated With Those of the Shipborne M-AERI". In: *IEEE Transactions on Geoscience and Remote Sensing* 59.12, pp. 9902–9913.
- 406
- 407 Madrigano, Jaime et al. (2015). "A case-only study of vulnerability to heat wave-related mortality in New York City (2000–2011)". In: *Environmental health perspectives* 123.7, pp. 672–678.
- 408
- 409 McEvoy, Darryn, Iftekhar Ahmed, and Jane Mullett (2012). "The impact of the 2009 heat wave on Melbourne's critical infrastructure". In: *Local Environment* 17.8, pp. 783–796.
- 410
- 411 Meir, Talmor et al. (2013). "Forecasting the New York City urban heat island and sea breeze during extreme heat events". In: *Weather and Forecasting* 28.6, pp. 1460–1477.
- 412
- 413 Melecio-Vázquez, David et al. (2018). "Thermal Structure of a Coastal–Urban Boundary Layer". In: *Boundary-Layer Meteorology* 169 (1), pp. 151–161. ISSN: 15731472.
- 414
- 415 Miller, STK et al. (2003). "Sea breeze: Structure, forecasting, and impacts". In: *Reviews of geophysics* 41.3.
- 416
- 417 Miralles, Diego G et al. (2014). "Mega-heatwave temperatures due to combined soil desiccation and atmospheric heat accumulation". In: *Nature geoscience* 7.5, pp. 345–349.
- 418
- 419 National Weather Service, NOAA (May 2018). *National Weather Service New York, NY excessive heat page*. URL: <https://www.weather.gov/okx/excessiveheat>.
- 420
- 421 NOAA et al. (1998). *Automated Surface Observing System (ASOS) User's Guide*. URL: <https://www.weather.gov/media/asos/aum-toc.pdf>.
- 422
- 423
- 424 Pelliccioni, A et al. (2012). "Some characteristics of the urban boundary layer above Rome, Italy, and applicability of Monin–Obukhov similarity". In: *Environmental fluid mechanics* 12.5, pp. 405–428.
- 425
- 426 Peng, Roger D et al. (2011). "Toward a quantitative estimate of future heat wave mortality under global climate change". In: *Environmental health perspectives* 119.5, pp. 701–706.
- 427
- 428 Pullen, Julie et al. (2007). "Atmospheric response to local upwelling in the vicinity of New York–New Jersey harbor". In: *Journal of applied meteorology and climatology* 46.7, pp. 1031–1052.
- 429
- 430 Quan, Jiannong et al. (2013). "Evolution of planetary boundary layer under different weather conditions, and its impact on aerosol concentrations". In: *Particuology* 11.1, pp. 34–40.
- 431
- 432 Ramamurthy, P and E Bou-Zeid (2017). "Heatwaves and urban heat islands: a comparative analysis of multiple cities". In: *Journal of Geophysical Research: Atmospheres* 122.1, pp. 168–178.
- 433
- 434 Ramamurthy, Prathap and E Bou-Zeid (2014). "Contribution of impervious surfaces to urban evaporation". In: *Water Resources Research* 50.4, pp. 2889–2902.
- 435
- 436 Robinson, Peter J (2001). "On the definition of a heat wave". In: *Journal of Applied Meteorology and Climatology* 40.4, pp. 762–775.
- 437
- 438 Rose, Thomas et al. (2005). "A network suitable microwave radiometer for operational monitoring of the cloudy atmosphere". In: *Atmospheric research* 75.3, pp. 183–200.
- 439
- 440 Sánchez, JL et al. (2013). "A method to improve the accuracy of continuous measuring of vertical profiles of temperature and water vapor density by means of a ground-based microwave radiometer". In: *Atmospheric Research* 122, pp. 43–54.
- 441
- 442 Shrestha, Bhupal et al. (2021). "Overview and Applications of the New York State Mesonet Profiler Network". In: *Journal of Applied Meteorology and Climatology* 60.11, pp. 1591–1611.
- 443
- 444

- 445 Stéfanon, Marc et al. (2014). "Soil moisture-temperature feedbacks at meso-scale during summer heat waves over
 446 Western Europe". In: *Climate dynamics* 42.5, pp. 1309–1324.
- 447 Tewari, Mukul et al. (2019). "Interaction of urban heat islands and heat waves under current and future climate
 448 conditions and their mitigation using green and cool roofs in New York City and Phoenix, Arizona". In:
 449 *Environmental Research Letters* 14.3, p. 034002.
- 450 Thomas, Natalie P et al. (2020). "Mechanisms associated with daytime and nighttime heat waves over the
 451 contiguous united states". In: *Journal of Applied Meteorology and Climatology* 59.11, pp. 1865–1882.
- 452 Thompson, William T, Teddy Holt, and Julie Pullen (2007). "Investigation of a sea breeze front in an urban envi-
 453 ronment". In: *Quarterly Journal of the Royal Meteorological Society: A journal of the atmospheric sciences,
 454 applied meteorology and physical oceanography* 133.624, pp. 579–594.
- 455 Wang, Z et al. (2012). "Lidar measurement of planetary boundary layer height and comparison with microwave
 456 profiling radiometer observation". In: *Atmospheric Measurement Techniques* 5.8, pp. 1965–1972.
- 457 Wu, Yonghua et al. (2019). "Observation of heat wave effects on the urban air quality and PBL in New York
 458 City area". In: *Atmospheric Environment* 218, p. 117024.
- 459 Yu, Yunyue et al. (2008). "Developing algorithm for operational GOES-R land surface temperature product". In:
 460 *IEEE Transactions on Geoscience and Remote Sensing* 47.3, pp. 936–951.
- 461 Zhang, Yuanjie et al. (2020). "Aircraft observed diurnal variations of the planetary boundary layer under heat
 462 waves". In: *Atmospheric Research* 235, p. 104801.
- 463 Zhao, Lei et al. (2018). "Interactions between urban heat islands and heat waves". In: *Environmental research
 464 letters* 13.3, p. 034003.
- 465 Zuo, Jian et al. (2015). "Impacts of heat waves and corresponding measures: a review". In: *Journal of Cleaner
 466 Production* 92, pp. 1–12.

467 **Appendix**

$$p = p_0 \exp \frac{-gz}{RT_0}$$

$$\theta = T \left(\frac{p_0}{p} \right)^{\frac{R}{cp}}$$

$$q = \frac{w}{1+w} = \frac{\frac{\varepsilon \rho'_v R_v T}{p - \rho'_v R_v T}}{1 + \frac{\varepsilon \rho'_v R_v T}{p - \rho'_v R_v T}}$$

$$Ri_b = \frac{g \Delta \bar{\theta}_v \Delta z}{\bar{\theta}_v [(\Delta \bar{U}^2) + (\Delta \bar{V}^2)]}$$

Table 2: Symbols and abbreviations used in the paper.

Symbol/Abbreviation	Definition
σ	Standard deviation
θ	Potential temperature
q	Specific humidity
U	Horizontal wind speed
w	Vertical velocity
UBL	Urban boundary layer
MLH	Mixed layer height

469 **Figures**

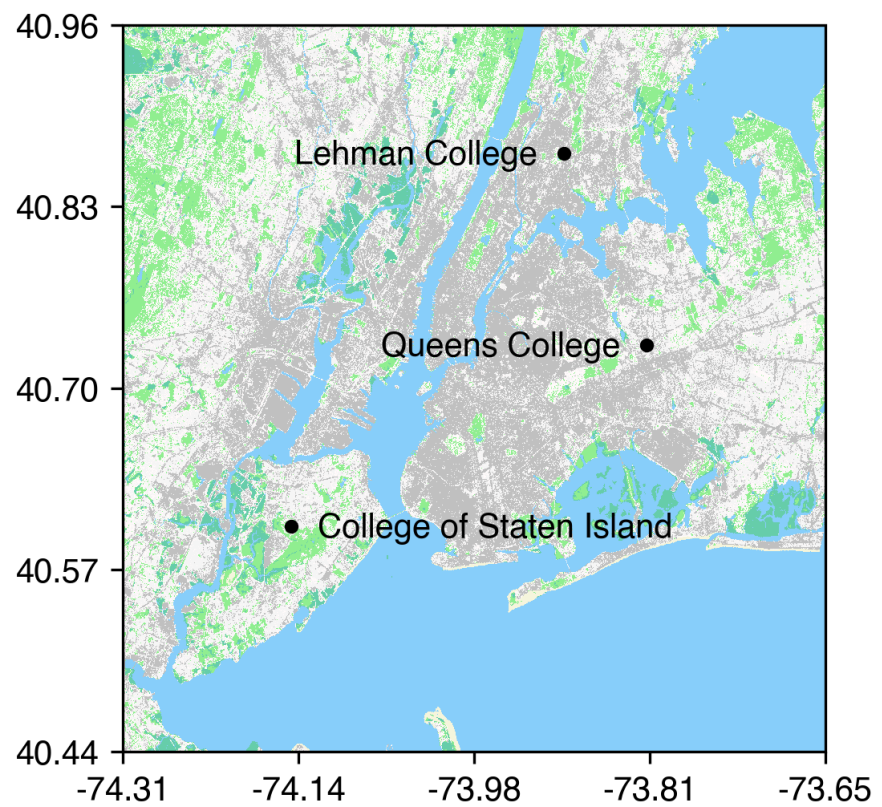


Figure 1: Observation sites overlaid on NLCD land cover types..

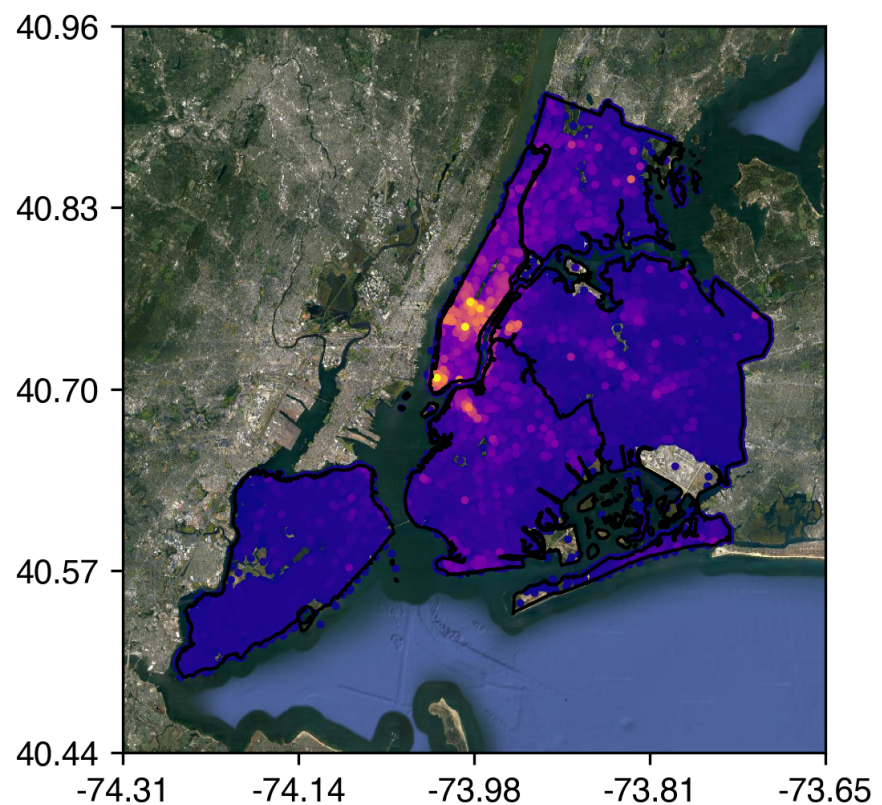


Figure 2: Building heights in New York City. Taken from NYC DOB data.

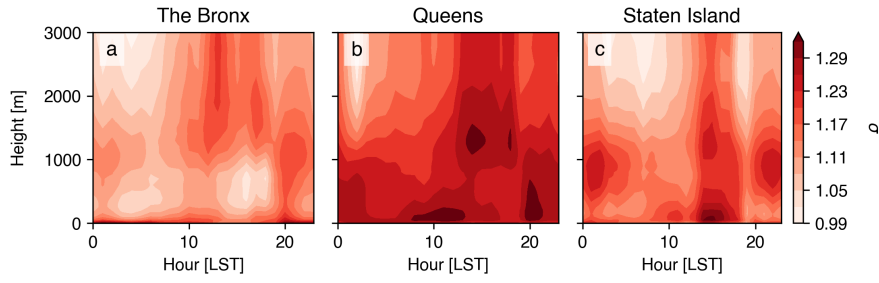


Figure 3: Anomalies of θ during extreme heat events relative to the climatology over the urban boundary layer.

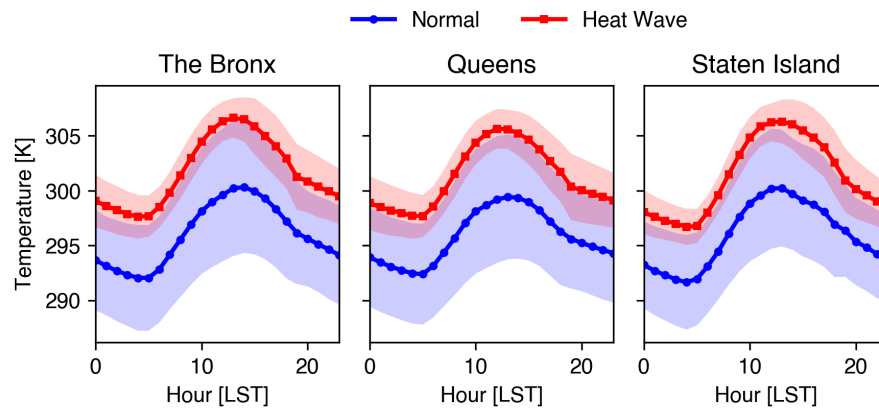


Figure 4: Anomalies of temperature during extreme heat events relative to the climatology at the surface.

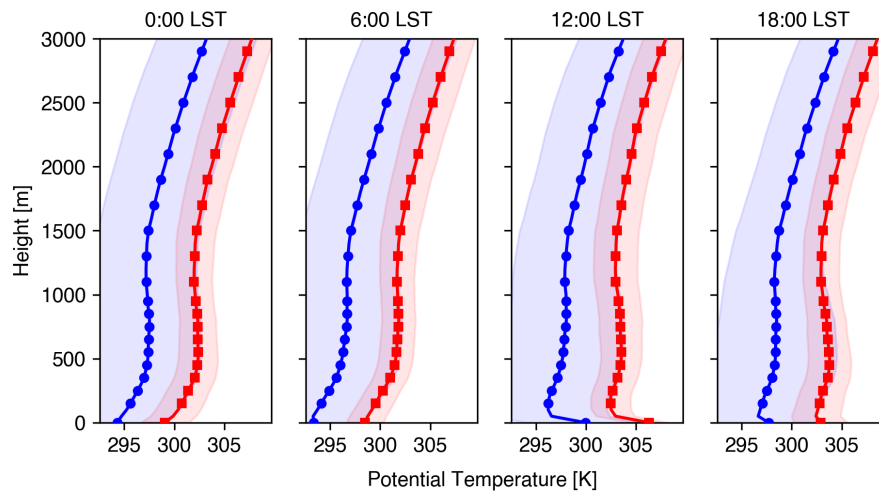


Figure 5: Vertical profiles of θ in the Bronx during normal days (blue) and extreme heat events (red).

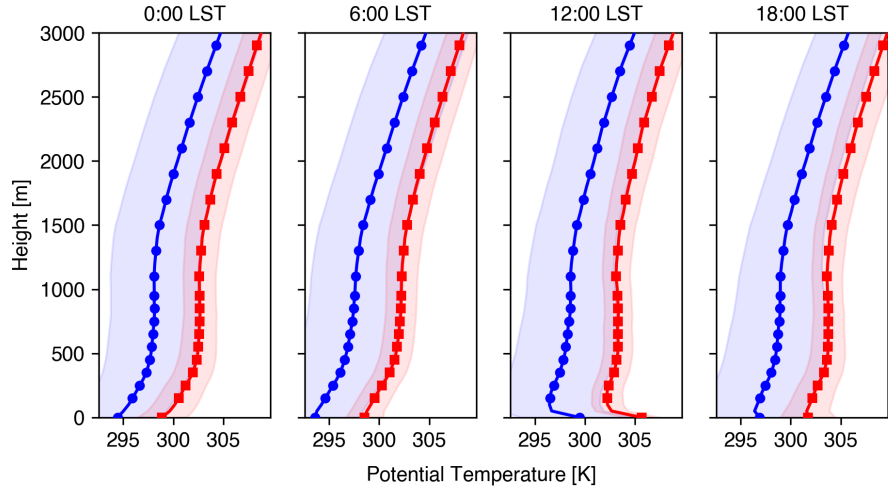


Figure 6: Vertical profiles of θ in Queens during normal days (blue) and extreme heat events (red).

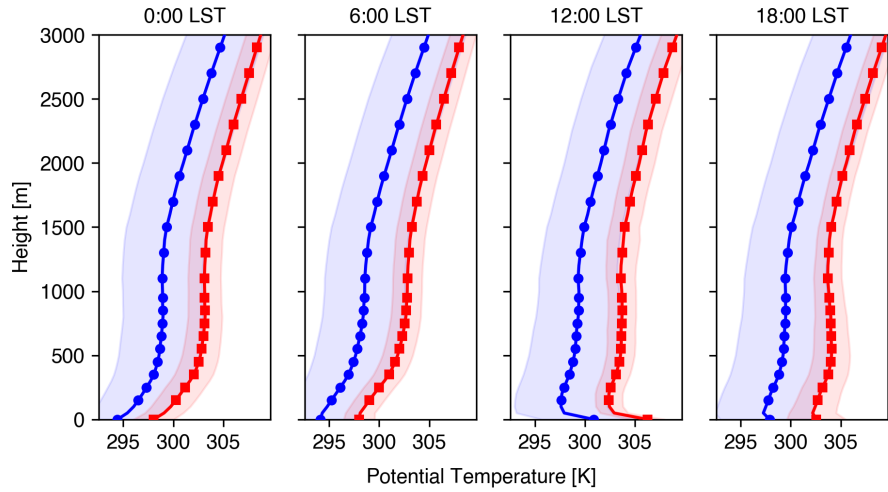


Figure 7: Vertical profiles of θ in Staten Island during normal days (blue) and extreme heat events (red).

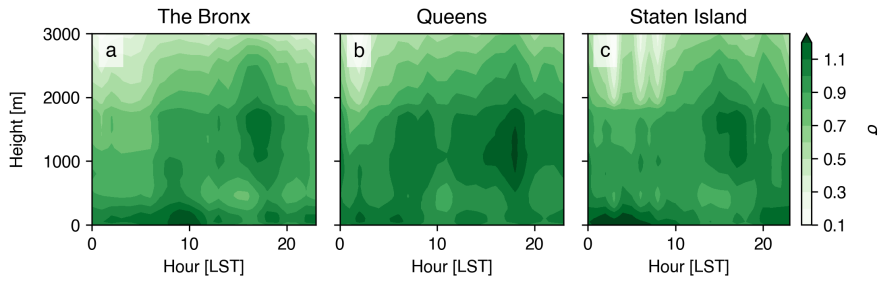


Figure 8: Anomalies of q during extreme heat events relative to the climatology over the urban boundary layer.

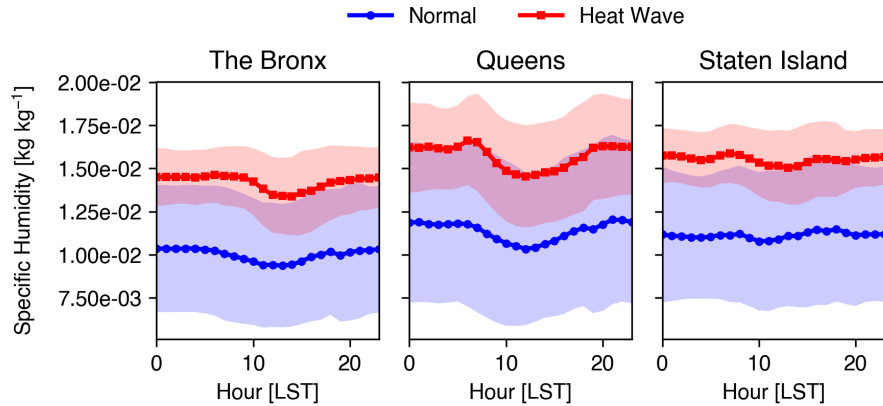


Figure 9: Anomalies of q during extreme heat events relative to the climatology at the surface.

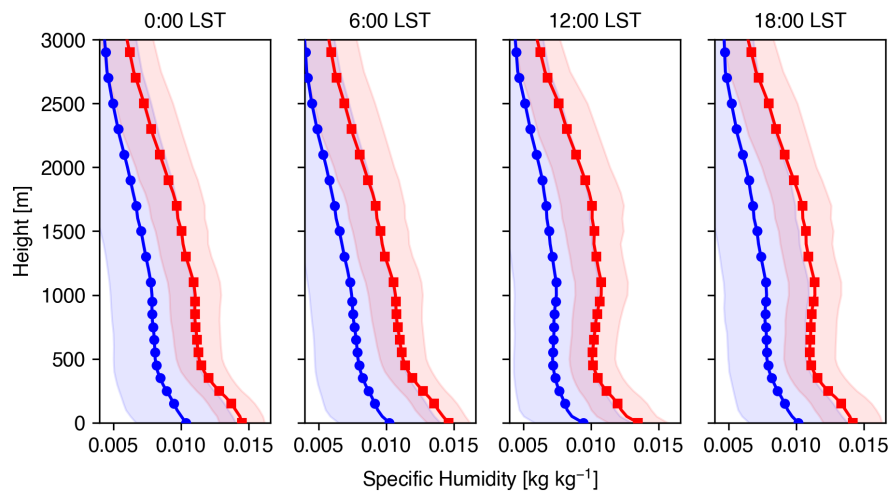


Figure 10: Vertical profiles of q in the Bronx during normal days (blue) and extreme heat events (red).

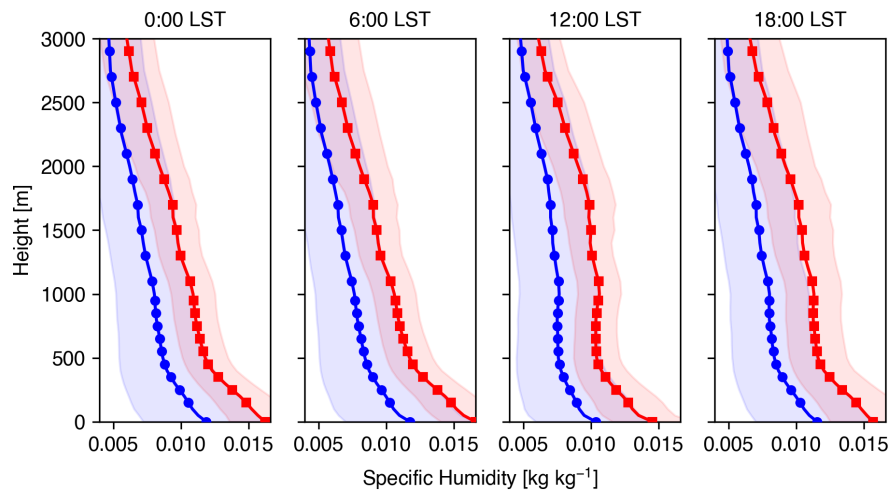


Figure 11: Vertical profiles of q in Queens during normal days (blue) and extreme heat events (red).

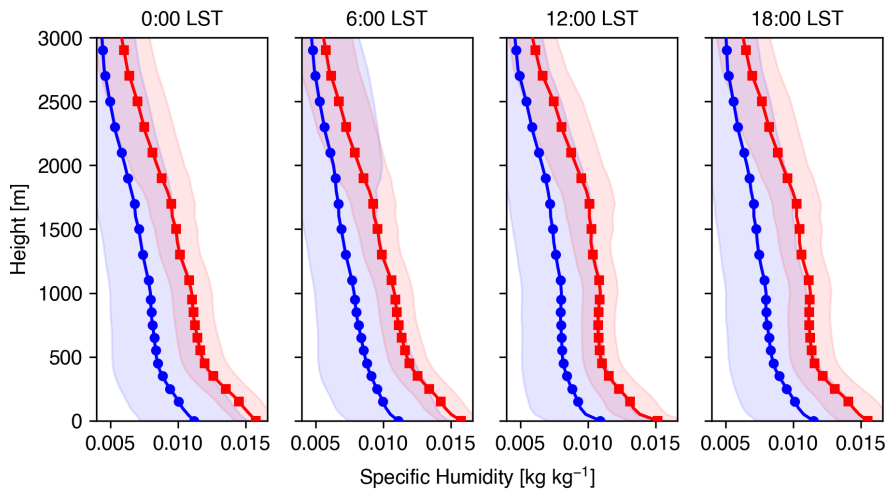


Figure 12: Vertical profiles of q in Staten Island during normal days (blue) and extreme heat events (red).

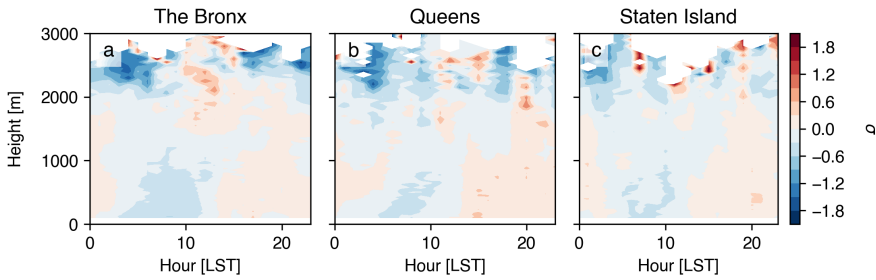


Figure 13: Anomalies of U during extreme heat events relative to the climatology over the urban boundary layer.

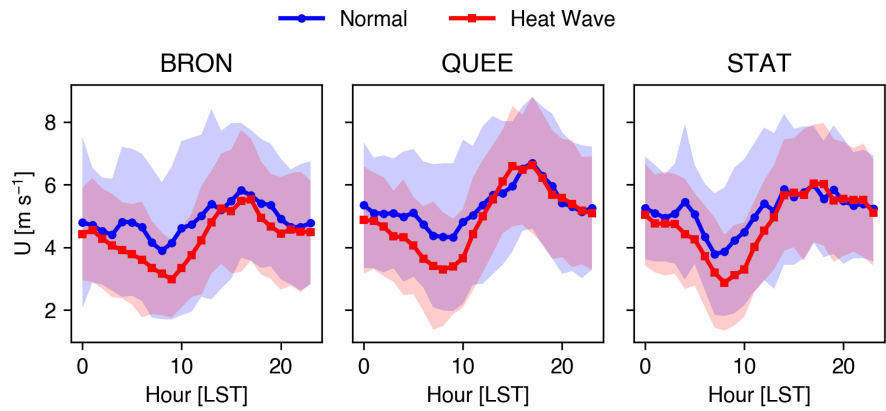


Figure 14: Anomalies of low-level U during extreme heat events relative to the climatology.

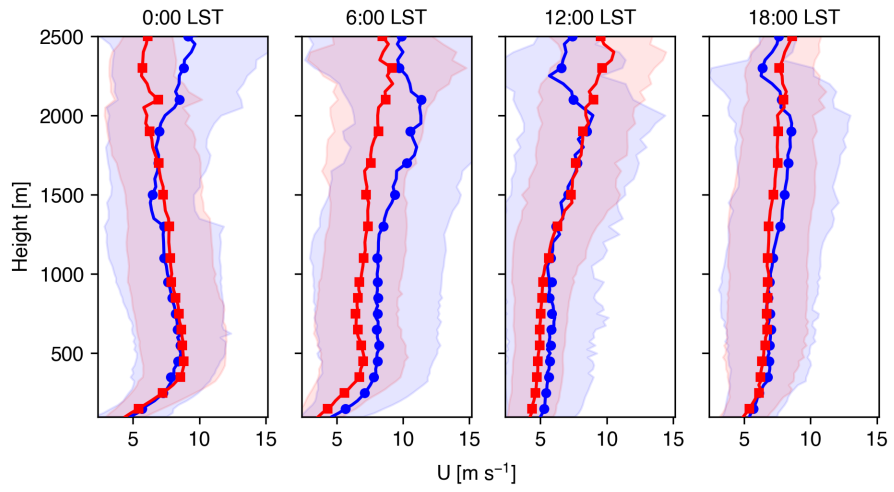


Figure 15: Vertical profiles of U in the Bronx during normal days (blue) and extreme heat events (red).

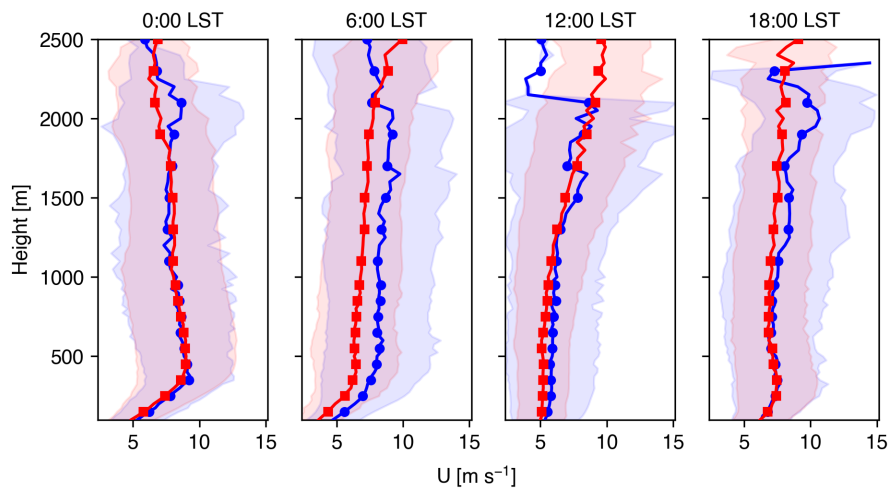


Figure 16: Vertical profiles of U in Queens during normal days (blue) and extreme heat events (red).

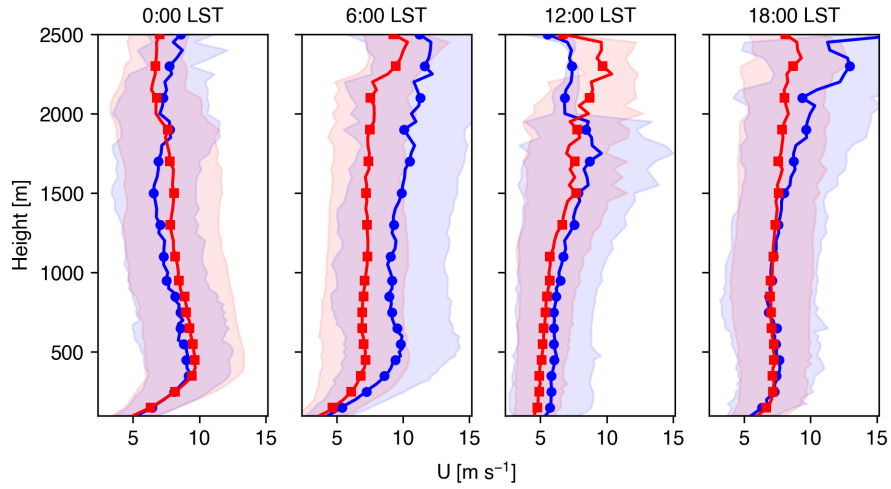


Figure 17: Vertical profiles of U in Staten Island during normal days (blue) and extreme heat events (red).

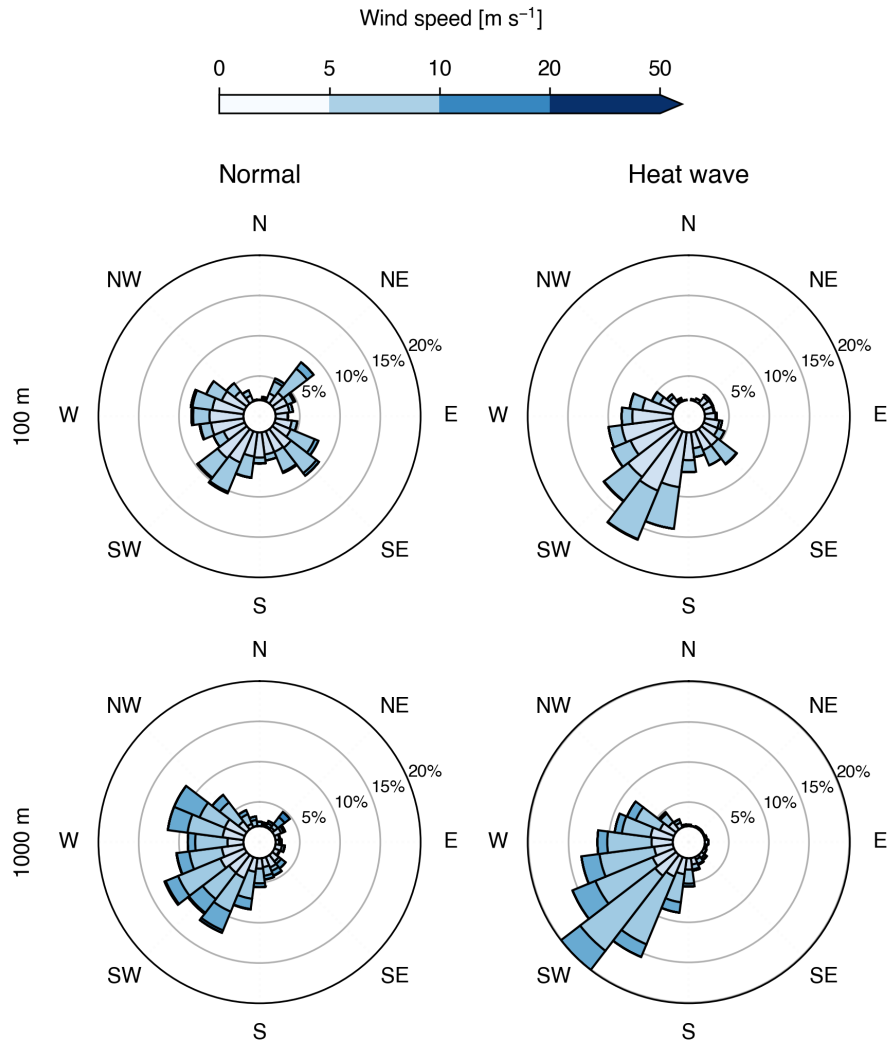


Figure 18: Horizontal winds in the lower-level (100 m) and mid-level of the urban boundary layer over the Bronx.

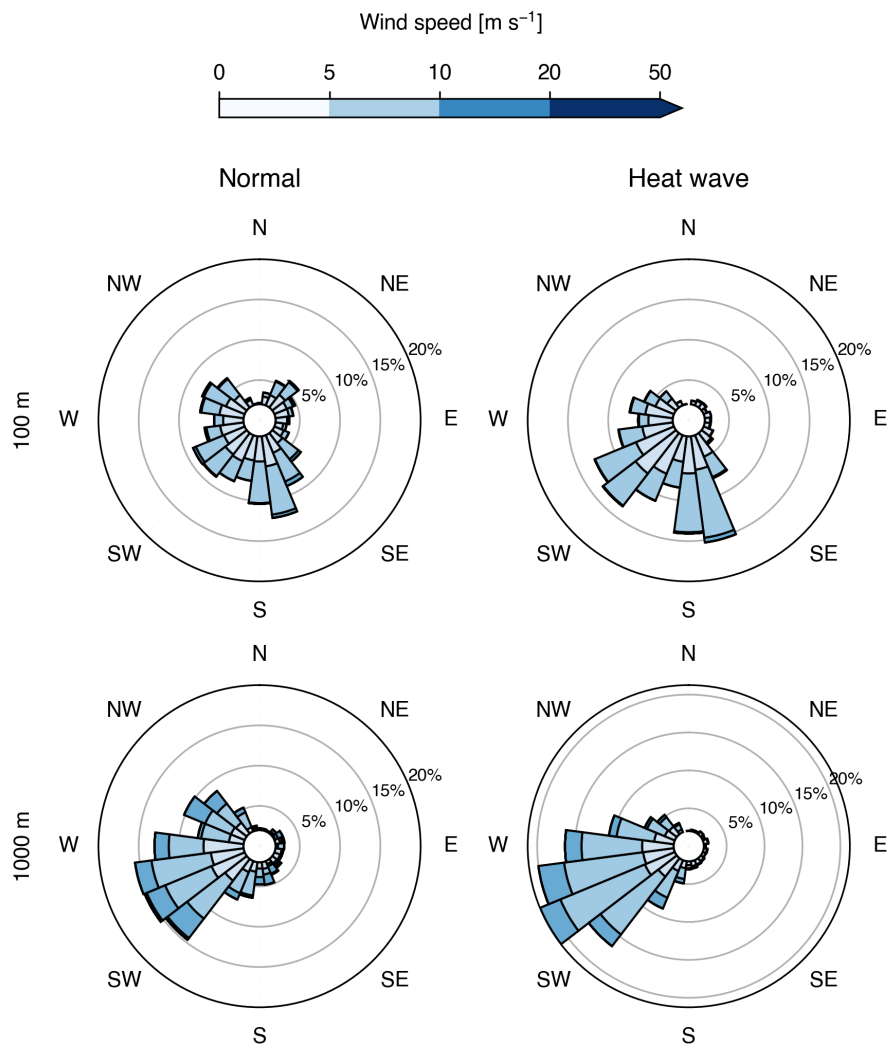


Figure 19: Horizontal winds in the lower-level (100 m) and mid-level of the urban boundary layer over Queens.

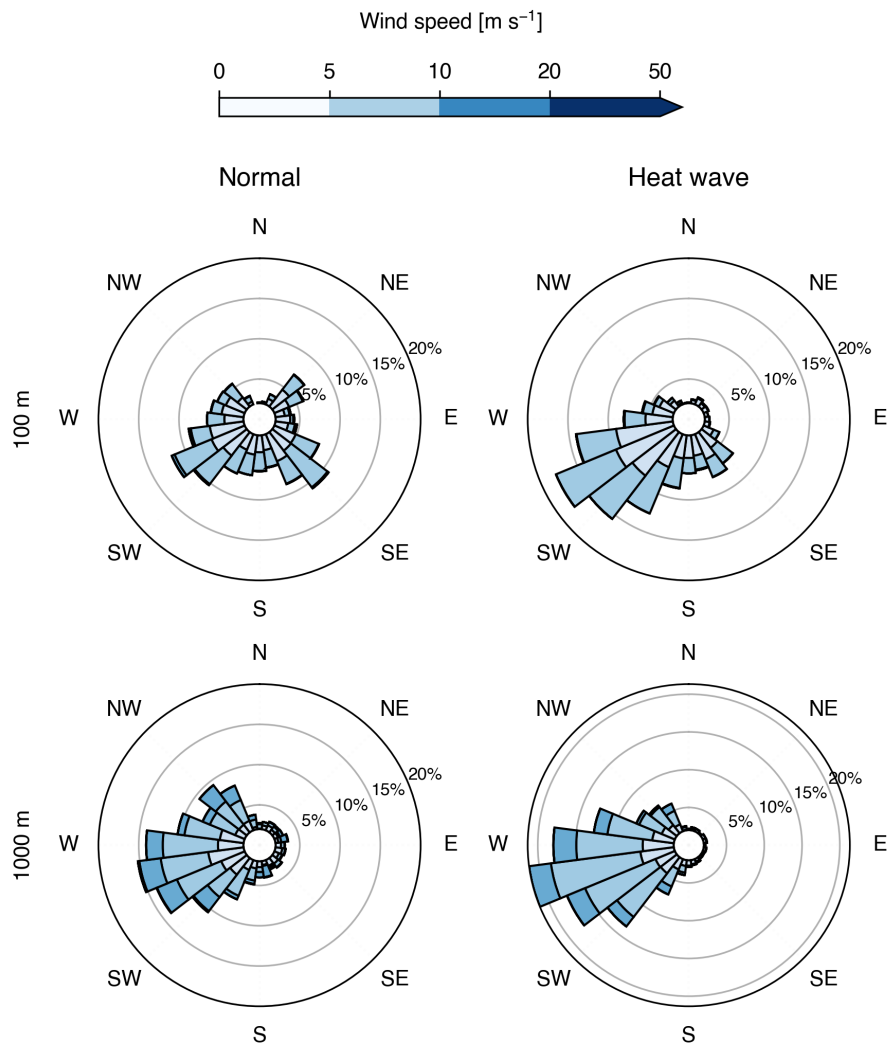


Figure 20: Horizontal winds in the lower-level (100 m) and mid-level of the urban boundary layer over Staten Island.

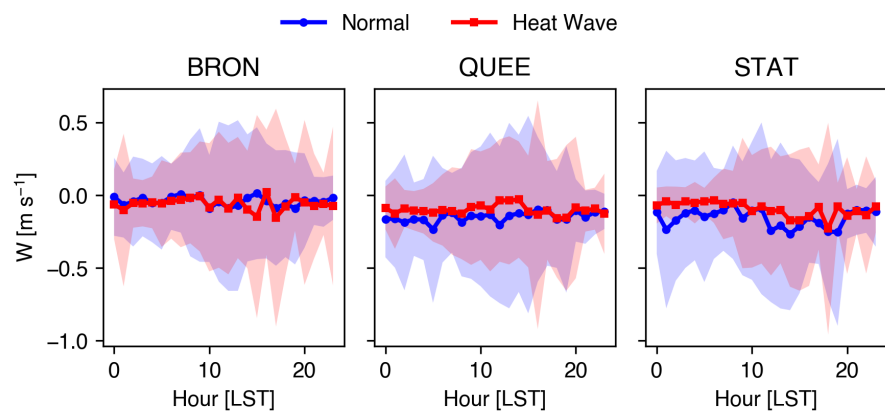


Figure 21: Anomalies of low-level w during extreme heat events relative to the climatology.

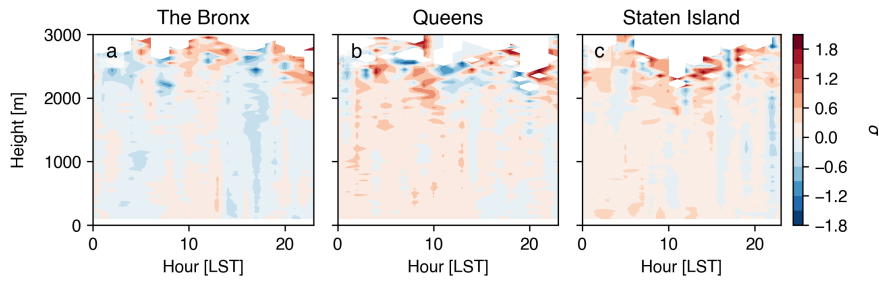


Figure 22: Anomalies of w during extreme heat events relative to the climatology over the urban boundary layer.

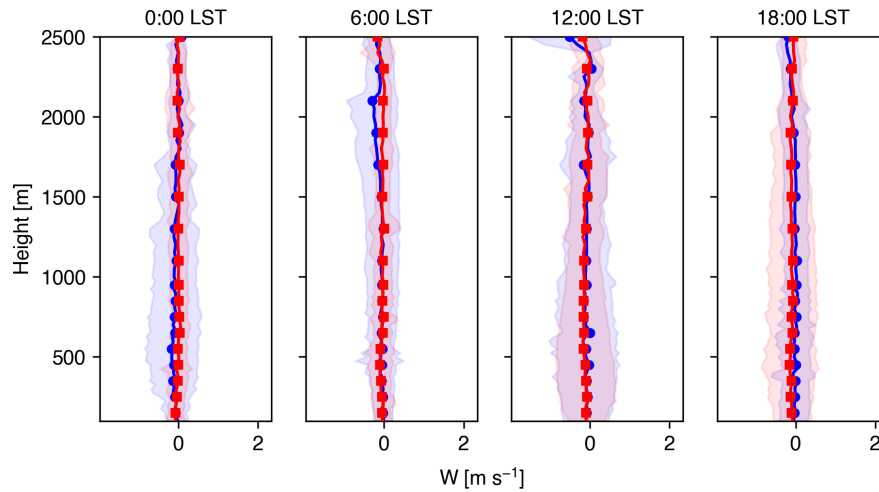


Figure 23: Vertical profiles of w in the Bronx during normal days (blue) and extreme heat events (red).

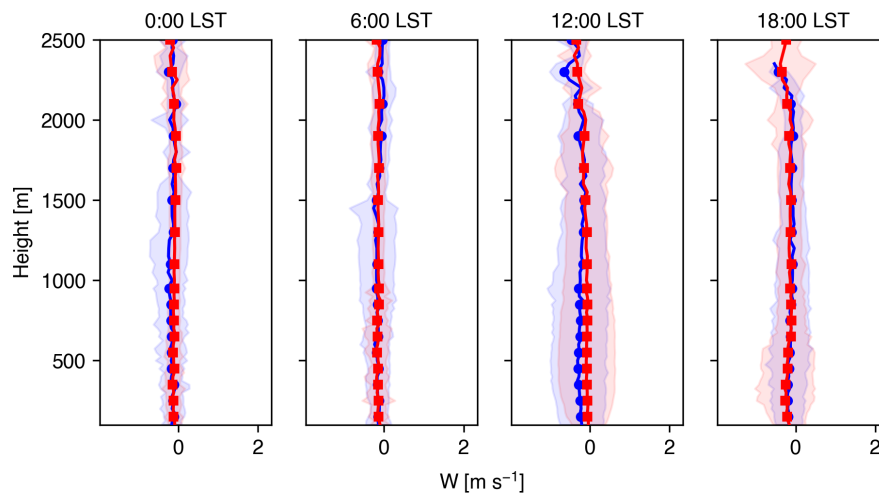


Figure 24: Vertical profiles of w in Queens during normal days (blue) and extreme heat events (red).

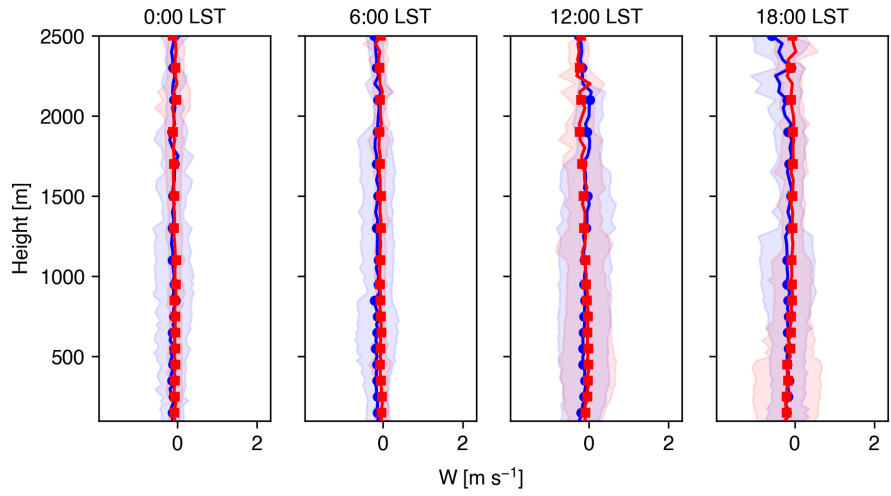


Figure 25: Vertical profiles of U in Staten Island during normal days (blue) and extreme heat events (red).

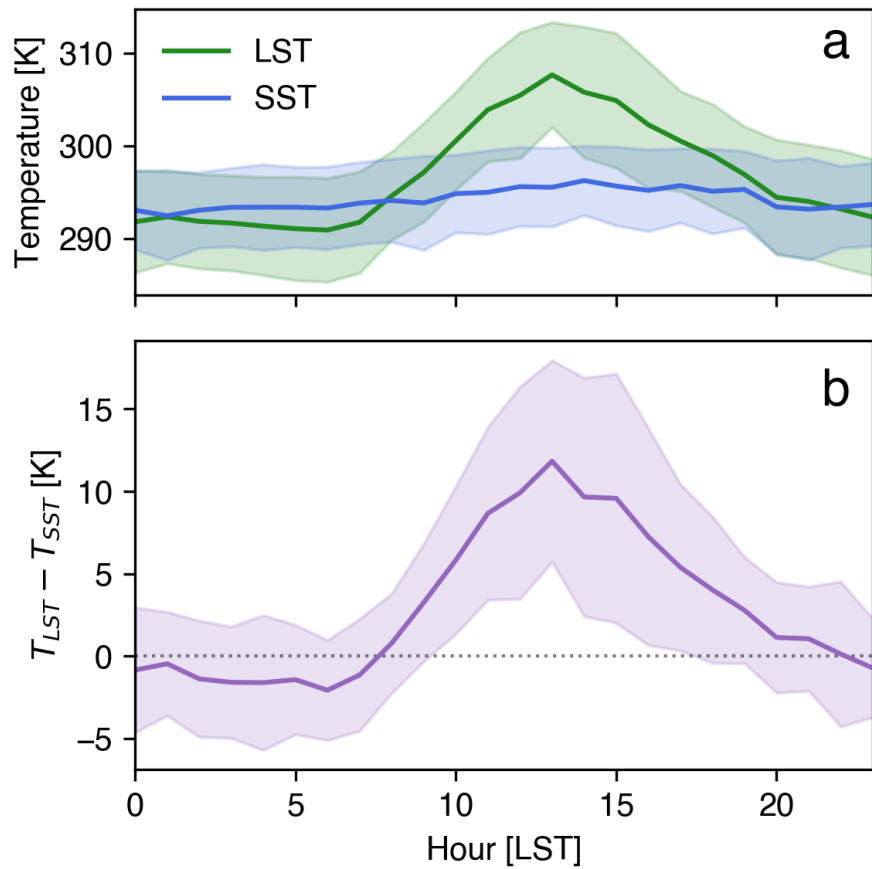


Figure 26: Temperature difference between Queens and New York Bight.

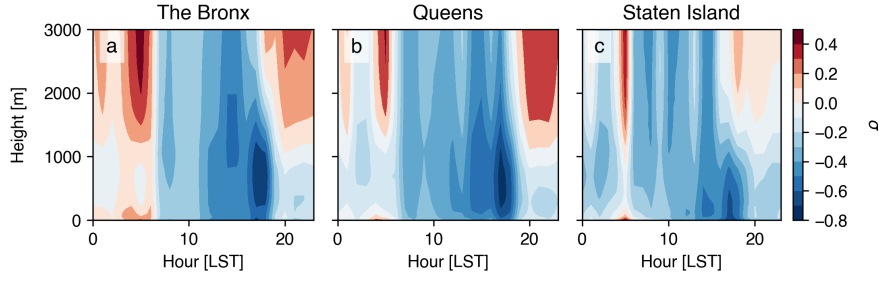


Figure 27: Anomalies of θ for normal days with a sea breeze relative to normal days without a sea breeze.

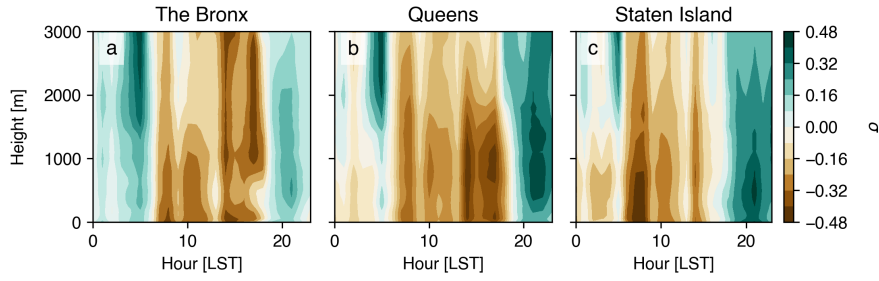


Figure 28: Anomalies of q for normal days with a sea breeze relative to normal days without a sea breeze.

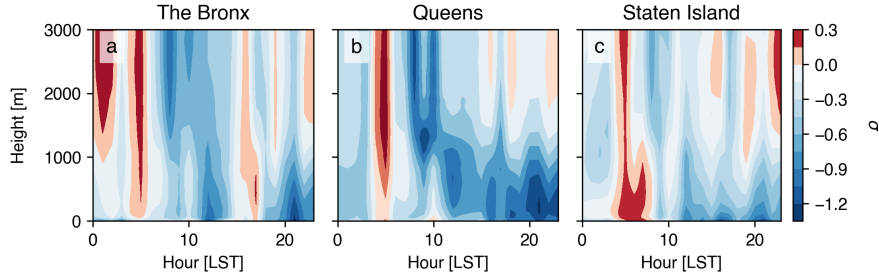


Figure 29: Anomalies of θ for heat wave days with a sea breeze relative to heat wave days without a sea breeze.

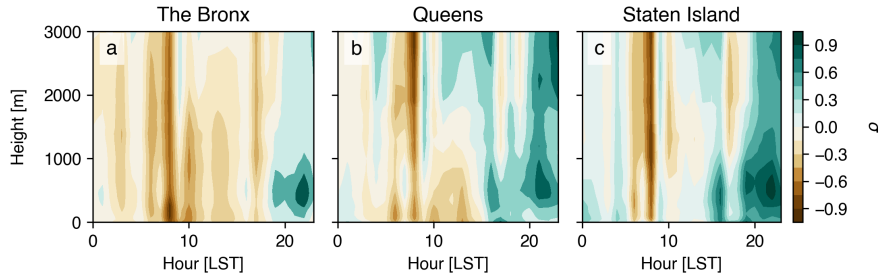


Figure 30: Anomalies of q for heat wave days with a sea breeze relative to heat wave days without a sea breeze.

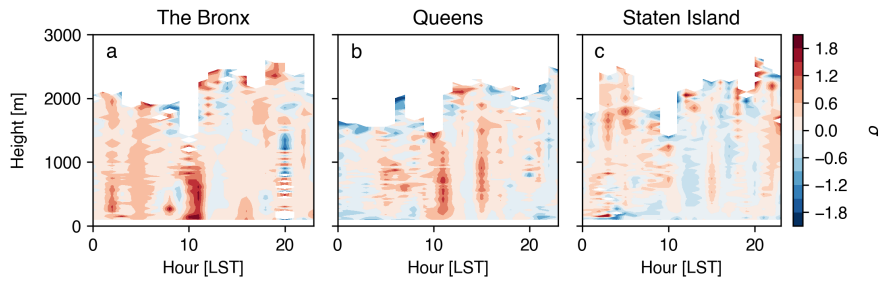


Figure 31: Anomalies of w for heat wave days with a sea breeze relative to heat wave days without a sea breeze.

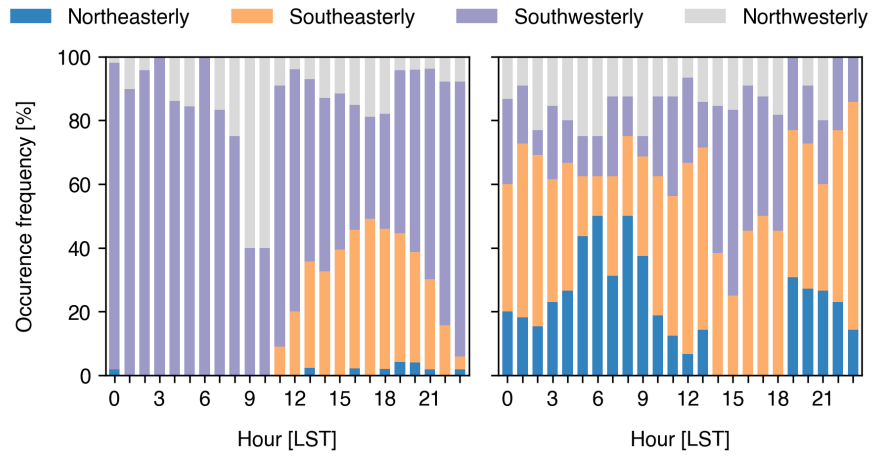


Figure 32: Occurrence frequency of wind directions at 100 m in the Bronx.

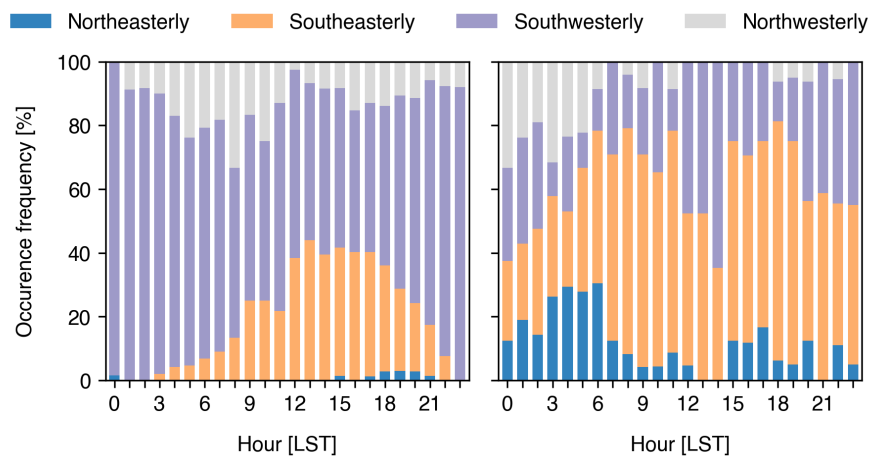


Figure 33: Occurrence frequency of wind directions at 100 m in Queens.

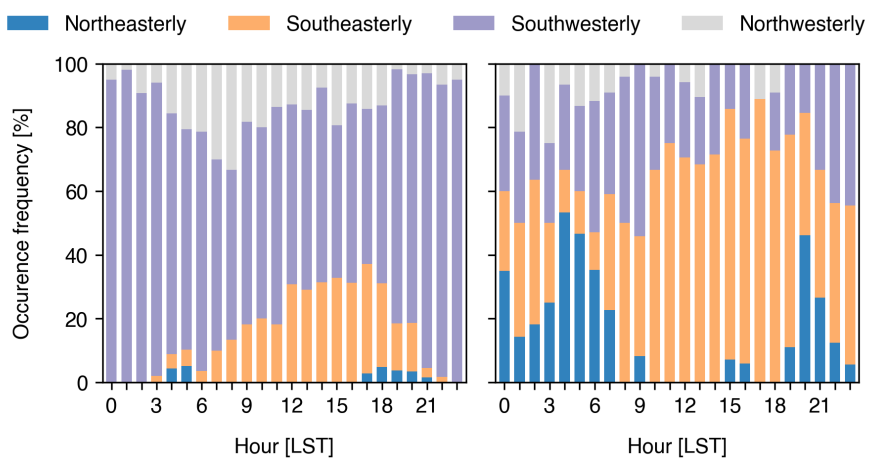


Figure 34: Occurrence frequency of wind directions at 100 m in Staten Island.